DOI: 10.1002/ejic.200800814

Influence of Surface Chemistry on Dehydrogenation in Carbon Cryogel Ammonia Borane Nanocomposites

Saghar Sepehri,[a] Betzaida Batalla García,[a] and Guozhong Cao*[a]

Keywords: Hydrogen storage / Nanoparticles / Carbon cryogel / Boron / Nitrogen / Mesoporous materials

This paper reports the synthesis and characterization of boron- and nitrogen-modified carbon cryogel (CC) ammonia borane (AB) nanocomposites (BNCC-AB) for hydrogen storage. Resorcinol–formaldehyde (RF) derived CCs were modified by homogeneous dispersion of AB in RF hydrogel prior to pyrolysis. Nanocomposites were fabricated by immersing CC in the AB solution. Nitrogen sorption analysis, X-ray photoelectron spectroscopy, and differential scanning calorimetry at multiple heating rates were used to study the structure and dehydrogenation properties of the nanocomposites. The results demonstrated lower dehydrogenation temperatures and reduced activation energies for AB when confined inside pores of B- and N-modified CCs relative to AB when confined in the unmodified CC with the same pore size.

Introduction

Amorphous porous carbon materials have attracted considerable attention for numerous applications because of their desirable properties, including high surface area, high pore volume, and tunable porous structures.[1–3] These materials can be made from carbonization of organic hydrogels generated by the sol–gel polycondensation of organic monomers in aqueous solution in the presence of a polymerization catalyst.[4] The organic hydrogels can be dried by different methods. Hydrogels dried by supercritical drying are called aerogels and those dried by freeze drying are called cryogels.[5] Carbon aerogels (CA) and carbon cryogels (CC) are interconnected porous carbon networks that are produced by pyrolysis of organic aerogels or cryogels, respectively. The final porous structure of the CAs and CCs depends on the synthesis and processing conditions and can be tailored to obtain desired pore sizes ranging from micropores (<2 nm) to mesopores (2–50 nm), and macropores (>50 nm).[1,6] Tailoring of the pore structure and doping of the carbon network can change the conductivity and catalytic activity of CA and CC and expand their applications.[7]

Recently, CAs and CCs have been studied as viable candidates to form carbon hydride nanocomposites for hydrogen storage with tunable dehydrogenation properties.[8] CAs and CCs are light-weight materials, and, therefore, they can show good gravimetric hydrogen density when used as a support for hydrides. Optimization of pore size and pore volume in CAs and CCs can provide better heat transfer and higher loading of the hydride. The confining of ammonia borane (AB NH_3BH_3) inside the pores of CCs has resulted in an appreciable reduction of the dehydrogenation temperature, improved reaction kinetics, and suppression of harmful by-products.[9] The use of neat AB results in the release of the first two moles of hydrogen in two steps at temperatures above 110 °C in exothermic reactions. The dehydrogenation temperatures depend on the heating rate.[10] For the practical application of AB as a hydrogen storage material for a polymer electrolyte membrane (PEM) fuel cell, the optimum decomposition temperature should be around 85 °C, which is the working temperature of PEM.[11] Enhanced dehydrogenation kinetics of AB inside CC may be attributed to the nanoscale effects of the CC matrix, which can increase the surface energy of the hydride as a result of the large surface to volume ratio; this results in lower dehydrogenation temperatures. Similar results have been observed for AB when milled or infused into mesoporous silica.[12] However, it is not known if the surface chemistry exerts a noticeable influence on the dehydrogenation process of hydrides that are confined inside nanopores.

In this study, we demonstrate that chemical modification of the surface of the pores in the CC can affect the dehydrogenation temperatures and kinetics of the hydride when confined in CC. Boron and nitrogen were introduced into the resorcinol–formaldehyde-derived hydrogels during solvent exchange by dissolving AB in *tert*-butyl alcohol. BN-modified CCs (BNCC) have been used as scaffolds for AB in BNCC-AB nanocomposites. The results show that confinement of AB into BNCC promotes the destabilization of AB and thus lowers its dehydrogenation temperature and activation energy relative to those of the unmodified CC scaffold with the same pore size.

[a] Department of Materials Science and Engineering, University of Washington,
302 Roberts Hall, Seattle, Washington 98195-2120, USA
Fax: +1-206-543-3100
E-mail: gzcao@u.washington.edu

Results and Discussion

XPS measurements of the cross section of RF-derived CC samples exhibit elemental and surface chemistry changes when B and N are introduced into the CC matrix (Table 1). The carbon content in the CC and BNCC is 99 and 93 atom-%, respectively. In BNCC, the oxygen content is significantly higher than that of CC. High resolution analysis reveals that the majority of the detected surface oxygen atoms (≈70%) are in the form of hydroxy groups. Moreover, the presence of B and N in BNCC is supported by the observation of 2 atom-% B and a very small N1s peak (about 0.1 atom-%). The low N to B ratio in BNCC and the high oxygen content in BNCC may indicate that N leaves the pyrolyzed sample and B is retained as B–OH. The measurements were performed on two spots of each sample (at the center and at the edge), and similar results were obtained, which is indicative of a uniform distribution of B and N in BNCC.

Table 1. Elemental distribution in the cross section of CC and BNCC.

Sample	C	O	B
CC (atom-%)	99	1	0
BNCC (atom-%)	93	5	2

Figure 1 shows the nitrogen sorption isotherms for the cryogels before and after pyrolysis. The isotherms for the unmodified cryogel (RF), BN-modified cryogel (BNRF), CC and BNCC samples are type IV isotherms with hysteresis associated with the dominance of mesoporosity.[6] However, BNRF shows a significantly lower pore volume as indicated by the low amount of nitrogen absorbed (Figure 1a), possibly as a result of the blocking of some of the pores by the introduction of AB to the gel. It is known that pyrolysis can lead to a decrease in the volume of the mesopores and to the emergence of micropores as a result of shrinkage,[1] as was detected for sample CC (Figure 1b, dashed line). However, the pore volume and surface area of the BNCC sample is significantly increased by pyrolysis (Figure 1b, solid line), which indicates less shrinkage in the mesopore region as a result of surface alteration.

The porous structure of the samples is detailed in Table 2. It can be seen that although the BET surface area (SA) of CC doubles after pyrolysis, only about half of the BET SA is related to the mesopores (≈57%, i.e. 253/446). For BNCC, on the other hand, there is ca. a 6-fold increase in the BET SA after pyrolysis, which mostly results from the increase in mesopore SA (≈86%, i.e. 246/285). Moreover, after pyrolysis, there is ca. an 8% decrease in the mesopore volume of CC, while that of BNCC is almost tripled. These observations indicate that the mesoporosity is improved in the BNCC sample. Pyrolysis introduces some microporosity in the CC sample, as expected; however, no micropores were detected in BNCC. These CC and BNCC samples exhibit similar pore sizes.

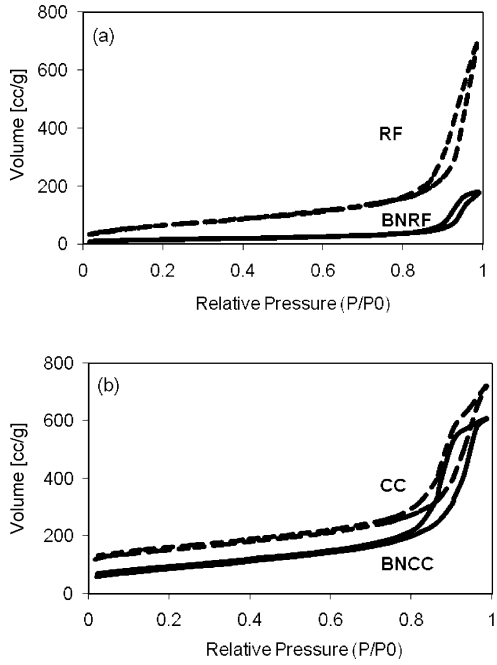

Figure 1. Nitrogen sorption isotherms for unmodified and modified cryogels (a) before pyrolysis: RF –dashed line, BNRF – solid line, (b) after pyrolysis: CC – dashed line, BNCC – solid line.

Table 2. Porosimetry data for RF hydrogels and carbon cryogels.

Sample	BET SA [m^2/g]	Meso SA[a] [m^2/g]	Micro SA [m^2/g]	Meso vol[a] [cc/g]	Micro vol[b] [cc/g]	Pore size[a] [nm]
RF	224	199	–	1.04	–	19.4
BNRF	50	48	–	0.27	–	19
CC	446	253	128	0.96	0.097	15.8
BNCC	285	246	–	0.89	–	15.6

[a] BJH desorption. [b] t-method.

Figure 2 shows that CC and BNCC have a similar pore size distribution in the mesoporous region, as obtained by applying the BJH method on the desorption curve of the BET isotherms.[13]

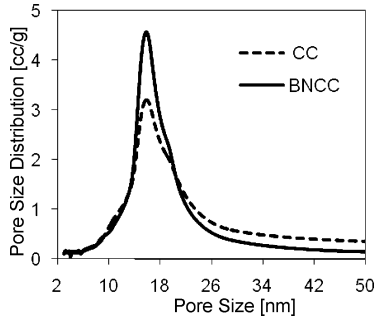

Figure 2. Pore size distribution of CC and BNCC (BJH desorption).

CC-AB and BNCC-AB nanocomposites were obtained by diffusing AB into CC and BNCC by soaking CC and BNCC in an AB/thf solution. The gaseous products from the thermal decomposition of neat AB and the nanocomposites were monitored by mass spectrometry. Hydrogen is the

main gaseous product formed from the decomposition of AB at the studied temperatures. Volumetric studies show that each mole of neat AB releases about 2 mol hydrogen (13 wt.-%). For the CC-AB and BNCC-AB nanocomposites, about 1.5 mol hydrogen (9 wt.-% of AB) was detected. It is likely that some hydrogen may be lost during the fabrication of nanocomposites at room temperature.[9] One of the undesirable volatile products from the dehydrogenation of AB is borazine, which can foul a fuel cell membrane and eventually render it unusable. The intensities measured for hydrogen and borazine at 50 °C (under vacuum) were used to calculate the ratio of borazine to hydrogen released from the decomposition of neat AB, CC-AB, and BNCC-AB (Figure 3). The intensity of hydrogen is normalized to one for each sample. The suppression of borazine in CC-AB and BNCC-AB nanocomposites is possibly due to its polymerization in the CC cavities at a rate faster than its escape into the gas phase.[9]

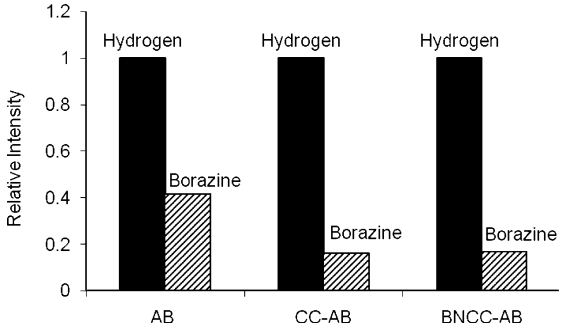

Figure 3. Relative intensity of borazine to hydrogen for neat AB, CCAB, and BNCCAB nanocomposites. The intensity of hydrogen is normalized to one for each sample.

Calorimetric measurements of the dehydrogenation of neat AB, CC-AB, and BNCC-AB nanocomposites were carried out by differential scanning calorimetry (DSC) at multiple heating rates of 2, 5, and 10 °C/min. At each rate, three runs were performed, and the observed peak temperatures (Table 3) were, in general, reproducible, with less than 1 °C difference. The dehydrogenation temperatures are lower for the nanocomposites than those for neat AB because of the large surface energy of nanosized AB in CC and BNCC. Moreover, lower dehydrogenation temperatures for BNCC-AB than those for CC-AB indicate faster dehydrogenation kinetics, which can be attributed to further destabilization of AB in BNCC-AB as a result of surface modification. It should be noted that the dehydrogenation temperatures reported here for CC-AB are higher than those in our previous report[8] because of the larger pore sizes of the CC samples used in this work.

Table 3. Peak temperatures for dehydrogenation of AB, CC-A, and BNCC-AB.

Heating rate [°C/min]	AB T_p [°C]	16 nm CC-AB T_p [°C]	16 nm BNCC-AB T_p [°C]
10	124	115	111
5	118	109	103
2	112	103	96

Figure 4 shows the DSC exotherms (at 5 °C/min) for the nanocomposites AB, CC-AB, and BNCC-AB. The thermal decomposition of AB shows an endothermic dip at approximately 105 °C (assigned to the melting of AB) and two exothermic maxima, one at approximately 115 °C and a smaller one at ca. 150 °C, which are associated with the release of first and second equivalent of hydrogen, respectively. These observations are in good agreement with those from the literature.[10] However, the DSC exotherms for CC-AB and BNCC-AB show two notable differences as compared to that of neat AB: first, the temperature for hydrogen release is lower (≈109 °C for CC-AB and ca. 103 °C for BNCC-AB, relative to 118 °C for AB). Further, there is only one exothermic peak, and no other peak is observed at temperatures as high as 160 °C.

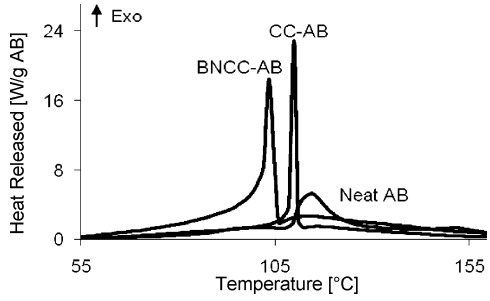

Figure 4. DSC exotherms for carbon cryogel AB nanocomposites and neat AB (heating rate 5 °C/min).

Activation energies were calculated for non-isothermal DSC runs with the Kissinger equation [Equation (1)]:[14]

$$\ln(\alpha/T^2) = -E_a/RT_p + \text{const} \quad (1)$$

where T_p is the peak temperature, $\alpha = dT/dt$ is the heating rate, and E_a is the activation energy. The plot of $\ln(\alpha/T_p^2)$ vs. $1/T_p$ is linear, and the slope of the resulting line corresponds to the values of the activation energies (Figure 5). The activation energy for release of the first equivalent of hydrogen from neat AB is found to be ca. 160 kJ/mol, which is comparable to the value reported in the literature.[15] The activation energies for the nancomposites are ca. 150 kJ/mol_{AB} and 115 kJ/mol_{AB} for CC-AB and BNCC-AB, respectively.

The lower dehydrogenation temperatures and activation energies of CC-AB and BNCC-AB can be attributed to the size-dependent surface energy of AB confined inside the nanoscale pores of CC and BNCC. The carbon matrix can reduce the distance for diffusion of hydrogen, increases the frequency of the reaction, which effectively accelerates the dehydrogenation process, and serves as an efficient pathway for heat transfer. Thus, the barrier to hydrogen release in CC-AB and BNCC-AB is lower. Moreover, the surface hydroxy groups may result in catalysis of the AB thermal reaction in the nanocomposites. Furthermore, the lower activation energy and dehydrogenation temperature in BNCC-AB than those of CC-AB can be attributed to the catalytic effect and not to nanoscale effects, since the porous structure (mesopore volume and pore size) of the CC and BNCC

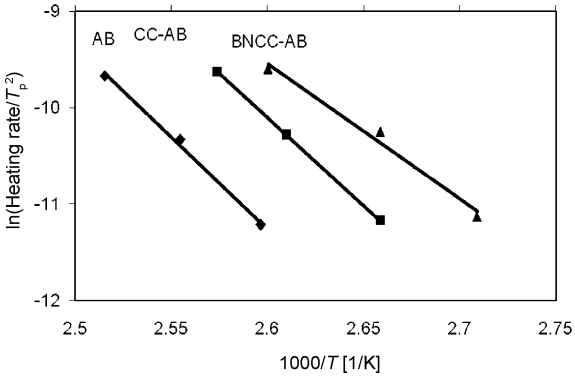

Figure 5. Kissinger plots for non-isothermal DSC runs at heating rates of 2, 5, and 10 °C/min. Activation energies are calculated from the slopes.

samples used in this study are very similar (Table 2). The presence of B and N and the excess of hydroxy groups on the surface BNCC (Table 1) can provide surface interactions that disrupt the dihydrogen bonding in AB and therefore lower the induction period for dehydrogenation and result in a lower barrier to hydrogen release in BNCC-AB than in CC-AB.

Conclusions

Modification of cyrogels with B and N has an appreciable impact on the porous structure of carbon cryogels and leads to a change in the surface chemistry. Nitrogen–boron-modified carbon cryogels (BNCC) were synthesized by homogeneous dispersion of ammonia borane (AB) in RF hydrogel during solvent exchange, followed by freeze drying and pyrolysis at elevated temperatures under nitrogen. This method results in the uniform distribution of B and N in the CC matrix whilst sustaining its porosity. Investigation of the hydrogen storage properties of the CC-AB and BNCC-AB nanocomposites shows that B and N modification of CCs further promotes the destabilization of AB and thus lowers its dehydrogenation temperature with reduced activation energy relative to that of the unmodified CC scaffold with the same pore size. These studies provide further experimental evidence that the dehydrogenation properties of hydrides can readily be controlled by the porous structure and surface chemistry of CC nanoscaffolds. A better understanding of the mechanisms of size confinement and surface interaction can be beneficial for the prediction and design of CC-hydride nanocomposites with the ability of tuning the dehydrogenation temperatures for specific applications.

Experimental Section

Fabrication: The chemicals utilized in this work are as follows: resorcinol (99+%, Sigma–Aldrich), formaldehyde solution (37 wt.-% in water, Fisher Scientific), sodium carbonate (99.5%, Sigma–Aldrich), trifluroacetic acid (99%, Sigma–Aldrich), *tert*-butyl alcohol (99.8%, J.T. Baker), tetrahydrofuran anhydrous (99.9%, Sigma–Aldrich), and AB (90%, Sigma–Aldrich), and were used as received. Resorcinol (R) was mixed with formaldehyde (F) solubilized in distilled water (W), with sodium carbonate as a catalyst (C). The R/W, R/C, and R/F ratios were kept at 0.035, 500, and 0.5 g/mL, respectively. The clear solutions were poured into glass vials (inner diameter = 10 mm) that were then sealed and cured at 90 °C for 7 d to complete the gelation process. The resulting RF hydrogels were washed with acid in ten times their volume with trifluroacetic acid solution (pH 1.9) at 45 °C for 3 d. The gels were put in fresh *tert*-butyl alcohol (ten times their volume) for solvent exchange (at room temperature for 24 h), repeating twice more with fresh solution. For the modified samples, AB was dissolved in *tert*-butyl alcohol used for the first solvent exchange step, and made as a 2 wt.-% solution. The gels, initially dark red in color, changed to light red during this step. The rest of the solvent exchange process was performed by using fresh *tert*-butyl alcohol to avoid precipitation of residual AB in the pores of the gels. The samples were freeze dried for a week under vacuum (at –50 °C) and pyrolyzed for 4 h at 1050 °C (heating rate 5 °C/min, nitrogen flow 25 mL/min). The CC-AB and BNCC-AB nanocomposites were obtained by soaking monolithic CC and BNCC samples in a solution of 10 wt.-% AB in tetrahydrofuran (99.9%, Sigma–Aldrich), under argon at room temperature for 3–5 h. The solvent was removed under vacuum. The sample weight gain {[(weight of AB loaded CC) – (weight of CC)] / (weight of CC)} for CC-AB and BNCC-AB was 50% and 60%, respectively.

Characterization: Elemental analysis was performed by X-ray photoelectron spectroscopy (XPS) on a thin slice of the samples, by using a Surface Science Instruments S-probe spectrometer (sampling depth about 50 Å, X-ray spot size 800 μm). The pore structure of the carbon cryogels was analyzed by means of nitrogen sorption (BET technique) at –196 °C by using a Quantachrome NOVA 4200e instrument. The specific surface area, and micropore and mesopore volumes were determined by using multipoint BET, t-method, and BJH (desorption) analyses, respectively. Dehydrogenation studies were performed by using a Netzsch 200 differential scanning calorimeter (DSC). Samples were heated to 200 °C at multiple heating rates under argon (flow rate 15 mL/min). Mass spectrometry measurements were performed and analyzed by a JEOL HX-110 mass spectrometer at discrete temperatures under vacuum.

Acknowledgments

This work was supported in part by National Science Foundation (DMI-0455994 and DMR-0605159) and Air Force Office of Scientific Research (AFOSR-MURI, FA9550-06-1-0326). This work was also supported by Washington Technology Center and EnerG2. XPS measurements were conducted at the University of Washington NESAC/BIO Surface Analysis Facility. The authors are very grateful to Dr. Tom Autrey from Pacific Northwest National Laboratory for his insightful comments.

[1] a) S. A. Al-Muhtaseb, J. A. Ritter, *Adv. Mater.* **2003**, *15*,101–114; b) Y. Yamamoto, T. Sugimoto, T. Suzuki, S. R. Mukai, H. Tamon, *Carbon* **2002**, *40*, 1345–1351.
[2] a) R. Petricevic, M. Glora, J. Frick, *Carbon* **2001**, *39*, 857–867; b) E. Frackowiak, F. Beguin, *Carbon* **2001**, *39*, 937–950.
[3] a) A. Feaver, G. Z. Cao, *Carbon* **2006**, *44*, 587–593; b) B. B. García, A. M. Feaver, Q. F. Zhang, R. D. Champion, G. Z. Cao, T. T. Fister, K. P. Nagle, G. T. Seidler, *J. Appl. Phys.* **2008**, *104*, 014305.

[4] R. W. Pekala, *J. Mater. Sci.* **1989**, *24*, 3221–3227.
[5] H. Tamon, H. Ishizaka, T. Yamamoto, T. Suzuki, *Carbon* **1999**, *37*, 2049–2055.
[6] K. S. W. Sing, D. H. Everett, R. A. W. Haul, L. Moscou, R. A. Pierotti, J. Rouquerol, T. Siemieniewska, *Pure Appl. Chem.* **1985**, *57*, 603–619.
[7] a) Z. H. Zhu, H. Hatori, S. B. Wang, G. Q. Lu, *J. Phys. Chem. B* **2005**, *109*, 16744–16749; b) R. Fu, M. S. Dresselhaus, G. Dresselhaus, B. Zheng, J. Liu, J. H. Satcher, T. F. Baumann, *J. Non-Cryst. Solids* **2003**, *318*, 223–232; c) S. Sepehri, B. B. García, Q. Zhang, G. Z. Cao, *Carbon*, in revision.
[8] a) A. F. Gross, J. J. Vajo, S. L. Van Atta, G. L. Olson, *J. Phys. Chem. C* **2008**, *112*, 5651–5657; b) A. M. Feaver, S. Sepehri, P. Shamberger, T. Autrey, G. Z. Cao, *J. Phys. Chem. B* **2007**, *111*, 7469–7472; c) S. Sepehri, B. B. García, G. Z. Cao, *J. Mater. Chem.* **2008**, *18*, 4034–4037.
[9] S. Sepehri, A. M. Feaver, W. J. Shaw, C. J. Howard, Q. Zhang, T. Autrey, G. Z. Cao, *J. Phys. Chem. B* **2007**, *111*, 14285–14289.
[10] a) F. Baitalow, J. Baumann, G. Wolf, K. Jaenicke-Rößler, G. Leitner, *Thermochim. Acta* **2002**, *391*, 159–168; b) T. B. Marder, *Angew. Chem. Int. Ed.* **2007**, *46*, 8116–8118.
[11] G. W. Crabtree, M. S. Dresselhaus, M. V. Buchanan, *Phys. Today* **2004**, *57*, 39–44.
[12] a) S. De Benedetto, M. Carewska, C. Cento, P. Gislon, M. Pasquali, S. Scaccia, P. P. Prosini, *Thermochim. Acta* **2006**, *441*, 184–190; b) A. Gutowska, L. Li, Y. Shin, C. M. Wang, X. S. Li, J. C. Linehan, R. S. Smith, B. D. Kay, B. Schmid, W. Shaw, M. Gutowski, T. Autrey, *Angew. Chem. Int. Ed.* **2005**, *44*, 3578–3582.
[13] M. Thommes in *Nanoporous Materials: Science and Engineering* (Eds: G. Q. Lu, X. S. Zhao), Imperial College Press, London, **2004**, vol. 4, pp. 317–364.
[14] H. E. Kissinger, *Anal. Chem.* **1957**, *29*, 1702–1706.
[15] F. H. Stephens, V. Pons, R. T. Baker, *Dalton Trans.* **2007**, 2613–2626.

Received: December 11, 2008
Published Online: January 14, 2009

